IEEE Robotics and Automation Letters (RA-L) paper, presented at ICRA 2026, Vienna, Austria. Cite as RA-L paper.

Safety-Critical Reactive Motion using Constrained Variable Admittance Control with Dual-Type Proximity Sensors

Seung Jae Moon[1], Hongsik Yim[1], Hyunchang Kang[1], Jae Yoon Shim[1], Dawoon Jung[2], and Hyouk Ryeol Choi[1,2], *Fellow, IEEE*

***Abstract*—We present a method that enhances the safety and responsiveness of robotic manipulators by employing constrained Variable Admittance Control (VAC) in conjunction with proximity perception. Recent studies have shown that manipulators equipped with proximity sensors can effectively avoid nearby obstacles in real-time. Nevertheless, unavoidable collisions remain a critical challenge in human-robot interaction (HRI). As a safety fallback, conventional reactive motion algorithms focus on obstacle avoidance but often suffer from inefficiency and disregard collision handling. Our approach integrates proximity-based pre-contact detection and VAC with QP-based motion constraints to proactively adjust impedance parameters while maintaining stable and controlled motion. By dynamically modulating stiffness and damping in response to sensor feedback, the system improves both obstacle avoidance performance and smooth contact handling. Additionally, a passivity-preserving energy tank mechanism mitigates instability arising from parameter variations, ensuring robust and adaptive behavior. Furthermore, experiments involving HRI[1] demonstrate that the proposed method ensures both safe avoidance and smooth contact handling. These results suggest that the proposed approach is highly applicable to safety-critical tasks in collaborative and industrial robotic environments.**

***Index Terms*—Reactive and Sensor-Based Planning, Proximity Sensor, Safety in HRI, Variable Admittance Control, Human-Centered Robotics.**

I. Introduction

As industrial robots expand beyond structured factory settings into dynamic environments, the demand for technologies that enable safe, real-time human-robot collaboration(HRC) has grown significantly [1]. Despite this demand, HRC is still largely confined to coexistence or sequential interaction, and true simultaneous cooperation remains elusive [2]. Genuine cooperation involves humans and robots working together in the same workspace, often requiring physical interaction to perform shared tasks. The absence of such cooperation diminishes both the efficiency and effectiveness of human-robot interaction (HRI), ultimately limiting the full potential of robotics. To address this challenge, the development of safe and reliable interaction technologies [2] is essential, as illustrated in Fig. 1.

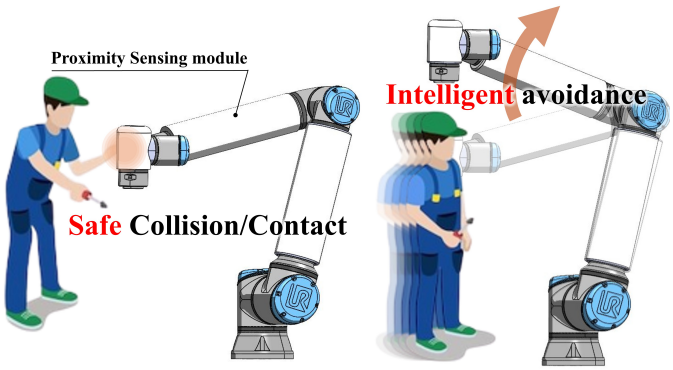

Fig. 1. Intelligent avoidance and safe contact using proximity sensor in real-time for safe HRI.

Traditional sensing methods, such as force/tactile sensors [3] and vision systems [4], have significantly contributed to safety for HRI [5]. However, force sensors lack pre-contact awareness necessary for proactive responses, while vision systems face limitations such as occlusions and difficulties in detecting transparent or dynamic objects, particularly in close-range scenarios. In contrast, proximity sensors—with low latency and skin-like properties—can provide rapid pre-contact information. Unfortunately, existing commercial proximity solutions [6] typically offer only basic responses (e.g., stopping the robot) and lack the ability to distinguish between humans and inanimate objects or to adapt dynamically to changing situations.

To address these limitations and enable seamless collaboration in shared workspaces, this study proposes a real-time safety-critical control system. Specifically, the approach introduces a novel reactive motion framework that utilizes dual-type proximity sensors [7], [8] to achieve real-time pre-contact detection and effectively differentiate between humans and inanimate objects. The sensors employed are radial-type, capable of measuring distances in the frontal region of each

Manuscript received: February 15, 2025; Revised April 29, 2025, Accepted June 21, 2025.

This paper was recommended for publication by Editor Kyung, Ki-Uk upon evaluation of the Associate Editor and Reviewers' comments.

This research was supported by a grant(No.P0026249) from International Cooperation in Industrial Technology (RD) Program funded by the Ministry of Trade, Industry and Energy (MOTIE, Korea).

[1]S.J. Moon, H. Yim, H. Kang, J. Shim, and H.R. Choi are with the School of Mechanical Engineering, Sungkyunkwan University, Seoburo 2066, Jangan-gu, Suwon, South Korea (e-mail: msj19@skku.edu; yimhongsik@skku.edu; gusckd0102@g.skku.edu; wodbs1118@g.skku.edu; hrchoi@me.skku.ac.kr).

[2]D. Jung and H.R. Choi are with AIDIN Robotics, 12-20, Simin-daero 327beon-gil, Dongan-gu, Anyang-si, South Korea (e-mail: dw.jung@aidinrobotic.co.kr; hrchoi@aidinrobotic.co.kr).

Digital Object Identifier (DOI): see top of this page.

[1]https://youtu.be/Vfs6Ow7X6XI

IEEE Robotics and Automation Letters (RA-L) paper, presented at ICRA 2026, Vienna, Austria. Cite as RA-L paper.

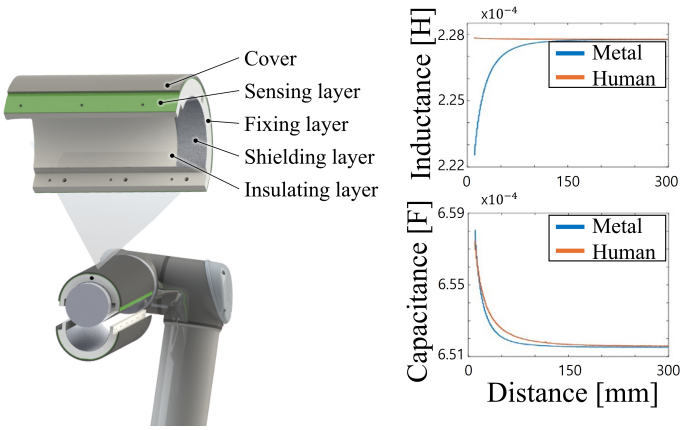

(a) (b)

Fig. 2. Dual-type proximity sensor (a) Sensor configuration (b) Sensing response, Capacitance increases as a human or metal object approaches, enabling distance measurement. Inductance decreases for metal but increases slightly for human presence, allowing for material discrimination.

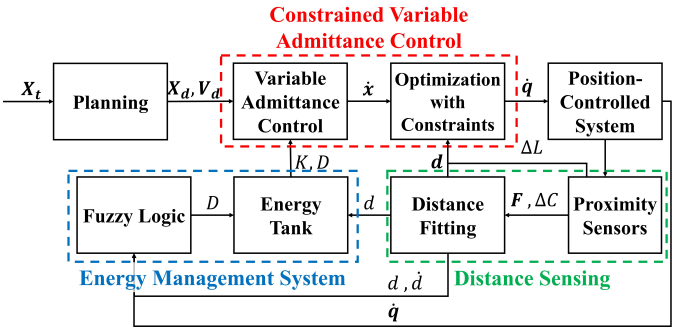

Fig. 3. Overview of the proposed control framework. The framework consists of three major components: constrained VAC, distance sensing, and energy management system. When an obstacle is detected, VAC generates a safer path, while the energy management system ensures stability and agility.

unit. They are arranged in an overlapping configuration around the robot's links, as illustrated in Fig. 2, thereby eliminating blind spots and ensuring comprehensive surface coverage. This setup enables the robot to respond dynamically and appropriately to various types of obstacles. Fig. 3 outlines the control framework, whose core is a constrained Variable Admittance Control (VAC) module, supported by energy tank mechanisms and fuzzy logic as auxiliary components. This integrated strategy overcomes the limitations of existing sensor technologies and control algorithms by enabling real-time pre-contact detection, scenario-adaptive responses, and effective impact mitigation—ultimately facilitating more advanced human-robot collaboration. Importantly, unlike prior methods, the proposed framework simultaneously addresses both obstacle avoidance and physical collision management.

The remainder of this paper is organized as follows. Section II reviews related work on reactive collision avoidance. Section III introduces variable admittance control integrated with energy tank mechanisms. Section IV explores the application of quadratic programming for safety-critical control. Section V presents experimental results and discussion. Finally, Section VI concludes the paper and outlines directions for future research.

II. Related Works

Reactive collision avoidance in robotics has progressed from vision-based approaches employing motion planning [9] to proximity sensor-based strategies that offer faster response times and reduced computational load [10]. These strategies can be broadly classified into the following categories:

1. Geometric Approaches:

Geometric methods are well-regarded for their precision in motion generation [11]. However, they are typically constrained by speed limits (e.g., a maximum of 150 mm/s) and are unable to fully exploit the real-time advantages offered by proximity sensors. Furthermore, they are less effective than vision systems in accurately representing the shapes of obstacles.

2. Jacobian-Type Approaches: These methods have gained popularity due to their adaptability and optimization capabilities. Maciejewski and Klein [12] introduced the concept of the "obstacle avoidance point Jacobian", which links joint velocities to obstacle point velocities:

$$\dot{\boldsymbol{x}}_{\boldsymbol{e}} = \boldsymbol{J}_{\boldsymbol{e}}\dot{\boldsymbol{q}}_{\boldsymbol{a}}, \quad \dot{\boldsymbol{x}}_{\boldsymbol{o}} = \boldsymbol{J}_{\boldsymbol{o}}\dot{\boldsymbol{q}}_{\boldsymbol{a}}. \tag{1}$$

Here, $\boldsymbol{q_a}$ and $\dot{\boldsymbol{q}}_{\boldsymbol{a}}$ represent the joint position and velocity vectors in the joint space. $\boldsymbol{x_e}$ and $\boldsymbol{x_o}$ denote the end-effector configuration and obstacle point in task space, respectively, while $\boldsymbol{p_o}$ is the closest point on the obstacle to the manipulator arm. Similarly, the obstacle Jacobian $\boldsymbol{J_o}$ relates the velocity of an obstacle point to the joint velocities.

By applying the inverse of $\boldsymbol{J_o}$, joint velocities corresponding to a desired trajectory relative to the obstacle point can be computed. This is analogous to using the (pseudo-)inverse of the end-effector Jacobian for task-space control. In collision avoidance, a natural choice is to generate motion away from the obstacle, as depicted by $\dot{x}_o$ in Fig. 4.

Building on this foundation, Ding et al. [13] demonstrated obstacle-overpassing motions using a 7-DoF robot equipped with proximity-sensing cuffs, thereby avoiding the local minima issues often encountered in potential field methods [9]. M'Colo et al. [14] employed capacitive sensors[2] to enable a sensing skin capable of avoiding both static and dynamic obstacles. However, these approaches frequently suffer from local minima, inefficient avoidance behavior, increased sensing and computational demands, or inability to reach the intended goal. Crucially, they often fail to distinguish between humans and inanimate objects, resulting in inefficient behaviors that are unsuitable for human-robot collaboration.

In response, recent studies have attempted to combine force control with optimization to improve either safety [15] or avoidance performance [16]. Moon et al. [16] further employed dual-type proximity sensors to enhance responsiveness and distinguishability. Nevertheless, critical limitations remain. Most existing approaches cannot distinguish humans from objects, resulting in slow and inefficient motions. Additionally,

[2]https://www.fogale-robotics.com/

IEEE Robotics and Automation Letters (RA-L) paper, presented at ICRA 2026, Vienna, Austria. Cite as RA-L paper.

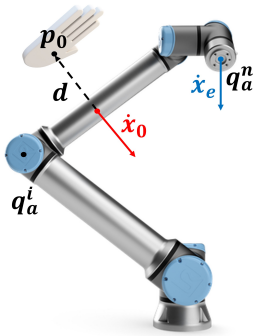

Fig. 4. Jacobian-type approach. When an obstacle approaches, a cartesian velocity vector $\dot{x}_0$ is generated in the opposite direction to the obstacle.

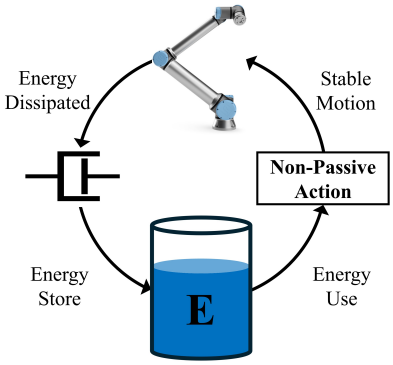

Fig. 5. Concept of energy tank. The resistance elements dissipate the robot's energy, which is then stored in the energy tank. The robot can perform non-passive actions while satisfying stability by utilizing the energy stored in the tank.

collision handling is either overlooked or treated separately from avoidance strategies [16]. These deficiencies underscore the need for reactive collision avoidance frameworks that integrate human-object distinction with collision management, thereby enabling both efficient and safe operation in dynamic environments.

In summary, although significant progress has been achieved, existing approaches often neglect integrated collision handling, human-object differentiation, and real-time efficiency. The present work aims to address these gaps and advance safer, more effective HRC.

III. Variable Admittance Control Using Energy Tank

To address the aforementioned challenges, we developed an obstacle avoidance and safety control algorithm suitable for real-world scenarios that explicitly accounts for collisions. This chapter introduces the VAC framework, which forms the foundation of the proposed Safety-critical Reactive Motion (Fig. 3). VAC enables simultaneous collision avoidance and impact mitigation through repulsive motion. In the following section, QP is integrated into the framework to enhance functionality, such as ensuring safe motion near singularities.

A. Variable admittance control

VAC is a force control method that adjusts the parameters of the mass (m), spring (k), and damper (d) according to the objective of the control [17]. While most studies vary m and d to improve direct teaching and interaction with environments [18], this work focuses on varying k and d to enhance real-time avoidance and collision-absorbing capabilities.

$$\begin{aligned}\boldsymbol{F_{ext}} =& \boldsymbol{M_d}(\boldsymbol{t})(\ddot{\boldsymbol{x}}_{\boldsymbol{d}} - \ddot{\boldsymbol{x}}_{\boldsymbol{0}}) + \boldsymbol{D_d}(\boldsymbol{t})(\dot{\boldsymbol{x}}_{\boldsymbol{d}} - \dot{\boldsymbol{x}}_{\boldsymbol{0}}) \\ &+ \boldsymbol{K_d}(\boldsymbol{t})(\boldsymbol{x}_{\boldsymbol{d}} - \boldsymbol{x}_{\boldsymbol{0}})\end{aligned} \tag{2}$$

Here, $\boldsymbol{M_d}$, $\boldsymbol{D_d}$, and $\boldsymbol{K_d}$ are positive matrices representing desired virtual inertia, damping, and stiffness, respectively, while $\boldsymbol{x}$, $\dot{\boldsymbol{x}}$, and $\ddot{\boldsymbol{x}} \in \mathbb{R}^6$ represent position, velocity, and acceleration vectors. $\boldsymbol{x_0} \in \mathbb{R}^6$ denotes the equilibrium position vector.

B. Passivity analysis with variable admittance control

Ensuring robot stability [19] is essential when modifying admittance parameters. Passivity, which ensures that energy is conserved within the system, is widely used to validate such stability [20]. Passivity implies that a system does not generate energy autonomously but instead behaves reactively to external input. In a spring-mass-damper system, the total mechanical energy can be expressed by a storage function:

$$V = \frac{1}{2}kx^2 + \frac{1}{2}mv^2 \tag{3}$$

Accordingly, the energy function of the VAC system is defined as a time-varying storage function:

$$\boldsymbol{V} = \frac{1}{2}\tilde{\boldsymbol{x}}^{\boldsymbol{T}}\boldsymbol{K_d}(\boldsymbol{t})\tilde{\boldsymbol{x}} + \frac{1}{2}\dot{\tilde{\boldsymbol{x}}}^{\boldsymbol{T}}\boldsymbol{M_d}(\boldsymbol{t})\dot{\tilde{\boldsymbol{x}}} \tag{4}$$

The rate of change of this storage function is given by:

$$\begin{aligned}\dot{\boldsymbol{V}} =& \tilde{\boldsymbol{x}}^{\boldsymbol{T}}\boldsymbol{K_d}(\boldsymbol{t})\dot{\tilde{\boldsymbol{x}}} + \frac{1}{2}\tilde{\boldsymbol{x}}^{\boldsymbol{T}}\dot{\boldsymbol{K}}_{\boldsymbol{d}}(\boldsymbol{t})\tilde{\boldsymbol{x}} + \dot{\tilde{\boldsymbol{x}}}^{\boldsymbol{T}}\boldsymbol{M_d}(\boldsymbol{t})\ddot{\tilde{\boldsymbol{x}}} \\ &+ \frac{1}{2}\dot{\tilde{\boldsymbol{x}}}^{\boldsymbol{T}}\dot{\boldsymbol{M}}_{\boldsymbol{d}}(\boldsymbol{t})\dot{\tilde{\boldsymbol{x}}}\end{aligned} \tag{5}$$

By applying the desired changes in stiffness and substituting Eq. 2, we derive the passivity condition as follows:

$$\dot{\boldsymbol{V}} = \dot{\tilde{\boldsymbol{x}}}^{\boldsymbol{T}}\boldsymbol{F_{ext}} + \left[\frac{1}{2}\tilde{\boldsymbol{x}}^{\boldsymbol{T}}\dot{\boldsymbol{K}}_{\boldsymbol{d}}(\boldsymbol{t})\tilde{\boldsymbol{x}} - \dot{\tilde{\boldsymbol{x}}}^{\boldsymbol{T}}\boldsymbol{D_d}\dot{\tilde{\boldsymbol{x}}}\right] \leq \dot{\tilde{\boldsymbol{x}}}^{\boldsymbol{T}}\boldsymbol{F_{ext}} \tag{6}$$

This condition ensures system stability by limiting internal energy changes induced by position errors.

C. Energy tank for manipulators

In prior work [16], VAC increased stiffness as a human approached the robot. While this improved responsiveness, it also elevated the risk of injury during collisions. In contrast, our approach reduces stiffness near obstacles to promote safer contact. However, restoring stiffness to its original value may compromise passivity. To overcome this limitation, we employ the energy tank method.

Ensuring user safety is critical in collaborative tasks. In admittance control, the control gains must be modulated to alternate between tracking and compliance modes. However,

IEEE Robotics and Automation Letters (RA-L) paper, presented at ICRA 2026, Vienna, Austria. Cite as RA-L paper.

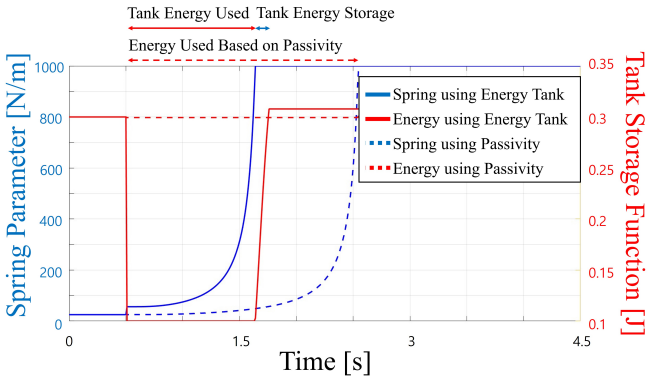

Fig. 6. Comparison between the energy tank method and conventional passivity approach. When restoring the spring constant to 1000, the energy tank method (solid line) is more efficient than the passivity method (dotted line) because it uses more energy to raise spring to 1000 faster.

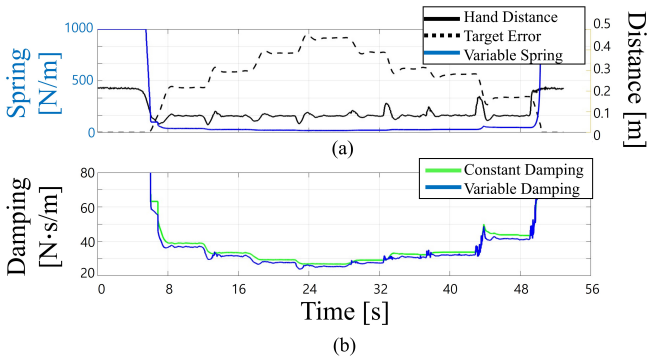

Fig. 7. Variable stiffness and Damping. (a) The hand approaches the robot, the robot is pushed away from its original position (black dotted line) and maintains a certain distance (black solid line) by variable spring. (b) Unlike when using a constant damping ratio, when using variable damping, the damping is lower when the robot is pushed away or maintained, and the damping ratio is higher when the hand moves away. This allows for both energy efficiency and avoidance performance to be achieved simultaneously.

such adjustments may disrupt passivity [21]. Energy tanks [22] provide a flexible mechanism for managing energy exchange. These tanks accumulate dissipated energy from sources such as damping, friction, and resistance, and strategically release it to support non-passive behavior when needed, such as rapid gain changes or post-impact recovery (Fig. 5). This mechanism enhances both system flexibility and stability in HRI.

Energy tanks have been utilized in diverse contexts, including passive inertia adaptation in admittance control [23] and stiffness modulation [21]. For example, [23] proposed a method that adjusts inertia to reduce user effort during physical HRI. While classical passivity conditions can be overly restrictive and degrade system performance [24], energy tanks offer a more relaxed framework by permitting parameter adjustments only when sufficient energy is stored.

In this work, we adopt a stiffness variation strategy for admittance-controlled robots that ensures flexibility while preserving passivity. The tank storage function from Eq. 6 is defined as:

$$T(e_t) = \frac{1}{2}e_t^2 \tag{7}$$

$$\dot{e_t} = \frac{\sigma}{e_t}\dot{\tilde{\boldsymbol{x}}}^{\boldsymbol{T}}\boldsymbol{D_d}\dot{\tilde{\boldsymbol{x}}} - \frac{\gamma}{e_t}\left(\frac{1}{2}\tilde{\boldsymbol{x}}^{\boldsymbol{T}}\dot{\boldsymbol{K}}_{\boldsymbol{d}}(\boldsymbol{t})\tilde{\boldsymbol{x}}\right) \tag{8}$$

Here, $T(e_t)$ represents the tank energy, and $\boldsymbol{e_t}$ denotes the tank state. The energy is bounded within $\delta \leq T(e_t) \leq \overline{T}$ to prevent excessive energy accumulation, which could lead to unstable behaviors. The upper bound is guaranteed by the parameters $\sigma \in$0,1 and $\gamma \in$0,1 that disable the energy storage in case a maximum, $\overline{T} \in R^+$ is reached. The bounding conditions are defined as:

$$\sigma = \begin{cases} 1 & if\ T(e_t) \leq \overline{T} \\ 0 & otherwise \end{cases} \quad \gamma = \begin{cases} \sigma & if\ \dot{K}_d(t) \leq 0 \\ 1 & otherwise \end{cases} \tag{9}$$

The derivative of the tank storage function is given by:

$$\dot{\boldsymbol{T}} = \boldsymbol{e_t}\dot{\boldsymbol{e_t}} = \sigma\dot{\tilde{\boldsymbol{x}}}^{\boldsymbol{T}}\boldsymbol{D_d}\dot{\tilde{\boldsymbol{x}}} - \gamma\left(\frac{1}{2}\tilde{\boldsymbol{x}}^{\boldsymbol{T}}\dot{\boldsymbol{K}}_{\boldsymbol{d}}(\boldsymbol{t})\tilde{\boldsymbol{x}}\right) \tag{10}$$

The total energy W of the system, combining the storage function T and the energy function V, is expressed as:

$$W = V + T \tag{11}$$

$$\begin{aligned}\dot{W} = \dot{V} + \dot{T} = \dot{\tilde{\boldsymbol{x}}}^{\boldsymbol{T}}\boldsymbol{F_{ext}} + \left[\frac{1}{2}\tilde{\boldsymbol{x}}^{\boldsymbol{T}}\dot{\boldsymbol{K}}_{\boldsymbol{d}}(\boldsymbol{t})\tilde{\boldsymbol{x}} - \dot{\tilde{\boldsymbol{x}}}^{\boldsymbol{T}}\boldsymbol{D_d}\dot{\tilde{\boldsymbol{x}}}\right] \\ +\sigma\dot{\tilde{\boldsymbol{x}}}^{\boldsymbol{T}}\boldsymbol{D_d}\dot{\tilde{\boldsymbol{x}}} - \gamma\left(\frac{1}{2}\tilde{\boldsymbol{x}}^{\boldsymbol{T}}\dot{\boldsymbol{K}}_{\boldsymbol{d}}(\boldsymbol{t})\tilde{\boldsymbol{x}}\right) \leq \dot{\tilde{\boldsymbol{x}}}^{\boldsymbol{T}}\boldsymbol{F_{ext}}\end{aligned} \tag{12}$$

If this inequality is satisfied, the energy tank enables passivity to be maintained more effectively than conventional conditions. As demonstrated in Fig. 6, using the Energy Tank results in faster recovery of the spring constant after a reduction. This allows the system to maintain stability and respond more effectively during dynamic interactions.

D. Admittance parameter control for obstacle avoidance and impact mitigation

In VAC, reducing stiffness decreases the internal energy of the system, thereby facilitating safer contact with humans or obstacles while maintaining passivity and stability. As shown in Fig. 6, decreasing stiffness does not require activation of the energy tank. However, increasing stiffness can violate passivity constraints, in which case the energy tank is employed to preserve stability.

The stiffness is modulated to maintain a safe distance from obstacles. Within a specified range, the stiffness is reduced based on proximity sensor measurements. Beyond this range, the spring constant is adjusted by incorporating both the measured distance and the position error. This strategy prevents oscillatory movements when the robot is pushed too far and minimizes collision risks when it is too close to an obstacle. As shown in Fig. 7, a consistent safety distance is maintained. The control law is defined as:

$$F_{ext} = k_d(x + \Delta d) \tag{13}$$

IEEE Robotics and Automation Letters (RA-L) paper, presented at ICRA 2026, Vienna, Austria. Cite as RA-L paper.

where x is the current distance to the target, and Δd represents an additional buffer distance that increases as a human approaches.

Unlike stiffness, damping (as defined in Eq. 4) does not directly affect energy flow and can be regulated independently of the energy tank. The damping coefficient d is proportional to both the mass and stiffness parameters ($d = \alpha\sqrt{mk}$), ensuring consistent motion. Nonetheless, the damping coefficient significantly impacts the energy recharge rate of the energy tank. By dynamically tuning the damping ratio, the system aims to improve agility when avoiding rapidly approaching obstacles and to accelerate energy recovery when obstacles move away.

To facilitate this adaptive control, a Mamdani-type fuzzy logic controller is implemented with three input variables and one output. The inputs are: obstacle distance (very close, close, normal), robot speed (safe, dangerous), and obstacle speed (approaching, receding). The output is the damping ratio, discretized into nine categories (very low, low, slightly low, mid-, mid, mid+, slightly high, high, very high), as illustrated in Fig. 8. The fuzzy controller is designed to achieve two primary objectives: enhancing agility in response to nearby or fast-moving obstacles and optimizing energy consumption when obstacles are distant or moving away. Damping is reduced when obstacles are close or when either the robot or the obstacle is moving quickly, thereby enabling rapid avoidance. Conversely, damping is increased when obstacles are far or receding, thereby promoting system stability and efficient energy management, as demonstrated in Fig. 7(b).

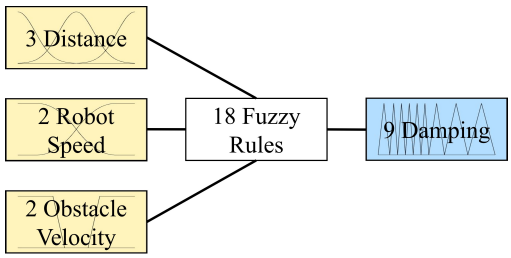

Fig. 8. Fuzzy logic for damping variation, 3 inputs(obstacle distance, obstacle speed, robot speed), 18 rules and 1 output(damping). When an obstacle is close or approaching, or the robot is in a fast situation with a high possibility of collision and needs to avoid quickly, lower the damping to improve avoidance performance; conversely, when the robot is slow and the obstacle is far or moving away, increase the damping to improve energy efficiency.

IV. Quadratic programming for safety control

The velocity generated by VAC is used as an input to compute an optimal motion that satisfies specific constraints. Unlike previous work [16], QP is applied after VAC to incorporate constraints such as velocity limits, ensuring safer and more efficient avoidance during collisions. The least-damped square method is used as the objective function:

$$\begin{aligned} g(\dot{\mathbf{q}}) &= \frac{1}{2}(\dot{\mathbf{x}} - \mathbf{J}\dot{\mathbf{q}})^\top(\dot{\mathbf{x}} - \mathbf{J}\dot{\mathbf{q}}) + \frac{\mu}{2}\dot{\mathbf{q}}^\top\dot{\mathbf{q}} \\ &= \frac{1}{2}\dot{\mathbf{q}}^\top(\mathbf{J}^\top\mathbf{J} + \mu\mathbf{I})\dot{\mathbf{q}} - \dot{\mathbf{x}}^\top\mathbf{J}\dot{\mathbf{q}} + \frac{1}{2}\dot{\mathbf{x}}^\top\dot{\mathbf{x}}. \end{aligned} \tag{14}$$

Here, $\dot{\boldsymbol{x}}$ represents the Cartesian velocity generated by VAC. The first term minimizes the quadratic error of the main task motion, while the second term damps joint velocities near singular configurations, preventing instability during collision avoidance.

A. Joint constraints

Joint constraints restrict the robot's joint positions $\boldsymbol{q}$ and velocities $\dot{\boldsymbol{q}}$ to predefined bounds:

$$\left.\begin{matrix} 0, & \mathrm{q} \le \mathrm{q}_{\mathrm{lb}} \\ \dot{\mathrm{q}}_{\mathrm{lb}}, & \text{otherwise} \end{matrix}\right\} \le \dot{\mathrm{q}} \le \begin{cases} 0, & \mathrm{q} \ge \mathrm{q}_{\mathrm{ub}} \\ \dot{\mathrm{q}}_{\mathrm{ub}}, & \text{otherwise} \end{cases} \tag{15}$$

Here, q_{lb}, q_{ub}, $\dot{q}_{lb}$ and $\dot{q}_{ub}$ denote the lower and upper bounds of joint positions and velocities. These bounds can be dynamically adjusted based on the robot's current state to prevent self-collision or limit joint movements within safe ranges.

B. Cartesian velocity constraints

Limiting Cartesian velocity $\dot{\boldsymbol{x}}$ ensures safe interaction with humans while maintaining efficiency when interacting with metals. Using the dual-type proximity sensor, the robot distinguishes between humans and metal, applying different velocity constraints. This approach not only reduces risk in human collisions but also ensures safe contact in intentional approaches. The allowable Cartesian velocity is reduced based on the detected distance:

$$\boldsymbol{J}\dot{\boldsymbol{q}} \le \dot{x}_s \tag{16}$$

$$\dot{x}_s = d_{min} \tag{17}$$

d_{min} is the shortest distance detected by the sensors, which determines the allowable Cartesian velocity $\dot{\boldsymbol{x}}$.

C. Joint acceleration constraints

To prevent abrupt changes in joint velocities caused by sudden object approach, joint acceleration constraints are applied:

$$\frac{\dot{\boldsymbol{q}}_{\boldsymbol{i}} - \dot{\boldsymbol{q}}_{\boldsymbol{i-1}}}{t} \le \boldsymbol{a} \tag{18}$$

Here, $\boldsymbol{a}$ is the acceleration maximum, $\dot{\boldsymbol{q}}\boldsymbol{i} - \mathbf{1}$ and $\dot{\boldsymbol{q}}\boldsymbol{i}$ are the previous and current joint velocities, and t is the control period. To avoid conflicts during QP solving, this constraint is applied post-optimization, ensuring smooth motion without compromising stability.

D. Obstacle avoidance constraints

VAC provides repulsive motion for obstacle avoidance, but without additional constraints, the robot may get trapped in local minima. To enhance avoidance performance, obstacle avoidance constraints are introduced. These restrict motion toward obstacles by dynamically adjusting the allowable velocity space. A linear inequality constraint restricts the allowed

IEEE Robotics and Automation Letters (RA-L) paper, presented at ICRA 2026, Vienna, Austria. Cite as RA-L paper.

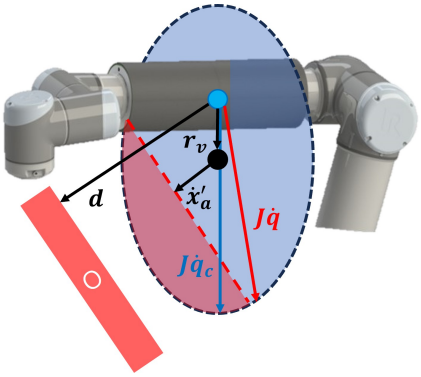

Fig. 9. Obstacle avoidance constraints illustrated in velocity space. The red zone indicates restricted motion directions. As the robot approaches an obstacle, the red zone expands to the maximum hemisphere. The entire sphere moves its center point in that direction according to the robot's current velocity.

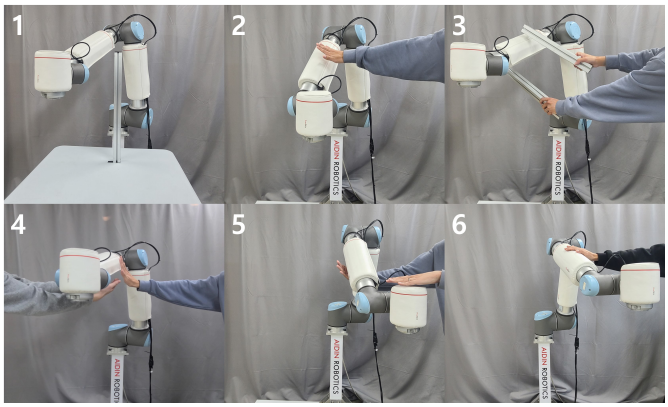

Fig. 10. Experimental scenarios: (1) static obstacle, (2) dynamic obstacle (human), (3) two metals at one link, (4) two humans at one link, (5) two hands at multiple links, (6) hand touch for contact safety evaluation.

avoidance motion x_d towards the direction d of the obstacle. It considers the robot's current velocity and shifts the velocity constraint sphere accordingly, releasing constraints in the direction of motion and tightening them in the opposite direction, as shown in Fig. 9.

$$\hat{\boldsymbol{d}}^{\boldsymbol{T}}\dot{\boldsymbol{x}} = \hat{\boldsymbol{d}}^{\boldsymbol{T}}\boldsymbol{J}\dot{\boldsymbol{q}} \leq \dot{\boldsymbol{x}}_{\boldsymbol{a}}^{'} + \hat{\boldsymbol{d}}^{\boldsymbol{T}}\boldsymbol{r}_{\boldsymbol{v}} \tag{19}$$

Here, $\boldsymbol{d}$ is the direction vector towards the obstacle, $\dot{\boldsymbol{x}}_{\boldsymbol{a}}^{'}$ is the constrained maximum velocity in the obstacle direction, and $\boldsymbol{r_v}$ is the vector from the robot to the sphere's center. Fig. 9 illustrates the dynamic adjustment of velocity constraints based on the obstacle's distance. The blue sphere is the set of velocity vectors that the robot can do, and the red part is the set of impossible vectors. All directions are treated equally if the robot's speed falls below a threshold.

V. Experiment Result

This section presents experimental results evaluating the proposed control strategy. Five algorithms were compared: VAC, VAC + Fuzzy, VAC + QP, VAC + QP + Fuzzy, and VAC + QP + Fuzzy with velocity constraints. Experiments were conducted with both metallic objects and human subjects to assess system performance under static and dynamic conditions, as shown in Fig. 10. All experiments were carried out using a commercially available robotic platform.

A. Experimental Setup

The experiments were performed using a UR10 robot (CB2 version). Eleven dual-type proximity sensors (capacitive and inductive) were installed on the robot—four on the forearm, four on the upper arm, two on the final wrist link, and one on the end cap, as illustrated in Fig. 10. The experimental parameters are summarized in Table I. These parameters were fine-tuned through preliminary trials to ensure both safety and performance during evaluation.

TABLE I
Experimental Setup Parameter

Parameter	Value	Unit
Sensor sampling rate	100.0	Hz
Robot Control Frequency	125.0	Hz
Maximum Robot Velocity(UR10 CB2)	1.0	m/s
Maximum sensor detection distance d_{max}	200.0	mm
Spring coefficient (k)	1000.0	N/m
Damping coefficient (d)	200.0	Ns/m
Mass coefficient (m)	10.0	kg
Energy tank range	0.1∼2.0	J
Maximum acceleration (a)	5.0	m/s^2
Desired maintained distance ($d_{desired}$)	100.0	mm

B. Experiments

Multiple experiments were conducted to assess the performance of the proposed method. The robot was assigned predefined poses and executed tasks such as pick-and-place using joint trajectory planning. The first experiment, shown in Fig. 10, focused on obstacle avoidance against a stationary metal object and compared the performance of each algorithm under this condition. This scenario simulated a situation in which a previously absent obstacle appears along the robot's path.

Fig. 11 shows the robot's avoidance behavior under each control strategy. The results are summarized as follows:

- VAC : This algorithm exhibited the most efficient trajectory for obstacle avoidance. However, collisions occurred due to its lack of additional safety constraints and the strong force directed toward the target, even at low speeds.

- VAC + Fuzzy : The addition of fuzzy logic allowed more agile responses by lowering damping. While it successfully avoided obstacles in many cases, collisions still occurred at higher speeds due to a lack of safety constraints.

- VAC + QP : Compared to VAC, this method produced a wider avoidance path. The added constraints helped prevent collisions and reduced excessive displacement, resulting in faster task completion. Nevertheless, occasional contact still occurred at higher speeds, causing slight shaking of the obstacle (see Table II). This suggests that a fixed damping ratio may limit adaptability.

- VAC + QP + Fuzzy Logic : As shown in the graphs and

IEEE Robotics and Automation Letters (RA-L) paper, presented at ICRA 2026, Vienna, Austria. Cite as RA-L paper.

TABLE II
TIME TO COMPLETE A GIVEN TRAJECTORY

V_{max}	VAC	VAC+Fuzzy	VAC+QP	Vac+Fuzzy+QP
	Time(s)			
0.3m/s	collision	5.96	5.89	5.88
1.0m/s	collision	collision	touch, 4.30	4.31

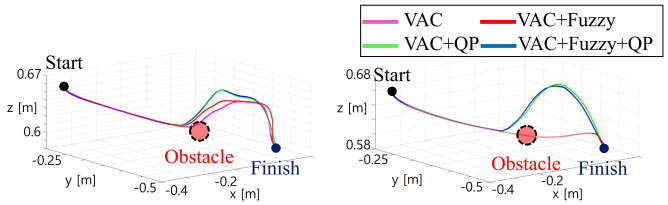

(a) (b)

Fig. 11. Obstacle avoidance in the presence of a static obstacle. (a) Robot speed 0.3m/s (b) Robot speed 1.0m/s. At slow speeds, only the VAC algorithm caused collisions, but at fast speeds, the VAC+fuzzy algorithm also caused collisions. In addition, the VAC+QP algorithm caused slight contact with the obstacle.

Table II, this algorithm avoided obstacles without contact and maintained high efficiency across speed conditions, demonstrating both robustness and adaptability.

The second experiment evaluated the algorithms' performance against dynamic obstacles, such as those encountered in HRI scenarios (see Fig. 10-2). In this setup, a human moved near the robot at varying speeds while the robot performed the same tasks as in the first experiment. The VAC + Fuzzy algorithm effectively avoided simple dynamic obstacles. However, as shown in the upper image of Fig.12, it occasionally failed to prevent collisions. In these cases (see also Fig. 13), the robot became trapped in a local minimum, resulting in persistent obstacle proximity and high tracking error. This was due to reliance on repulsive motion alone. In contrast, the VAC + QP + Fuzzy algorithm successfully avoided dynamic obstacles and reached the target poses without collisions.

The next experiment investigated more complex scenarios involving two obstacles approaching simultaneously at one link, as shown in Fig. 10-3,4. Only the VAC+QP+Fuzzy algorithm was evaluated, excluding methods that failed in prior tests. In the first scenario, two metal objects approached the same link. Fig. 14 (a) demonstrates that the algorithms effectively avoided both obstacles without collision. When interacting with humans, Cartesian velocity constraints slowed motion but significantly improved safety, even in the event of contact.

In Fig. 10-5, two obstacles approached separate links of the robot. The robot successfully avoided at all links, as shown in Fig. 14 (b). Without velocity constraints, avoidance was quicker; with limits, avoidance was slower but safer.

The final experiment (Fig. 10-6) evaluated whether a human could safely make contact with the robot, an essential aspect of safe HRI. As shown in Fig. 15, the robot rapidly decelerated before contact, adjusting its velocity based on human proximity. The velocity reached zero at the moment of contact. Additionally, Fig. 16 presents survey results on participants' perceived fear and softness during interaction. Most participants reported that the robot felt non-threatening

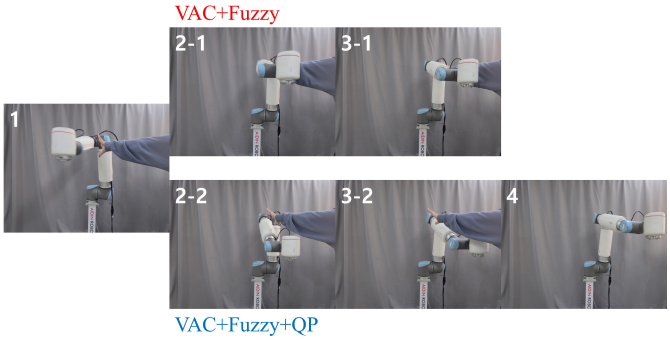

Fig. 12. Comparison of VAC+Fuzzy and VAC+QP+Fuzzy with dynamic obstacles. VAC+Fuzzy algorithm failed to avoid the obstacle blocking the path and was stuck in the local minia. VAC+Fuzzy+QP algorithm avoided the obstacle blocking the path and reached the target.

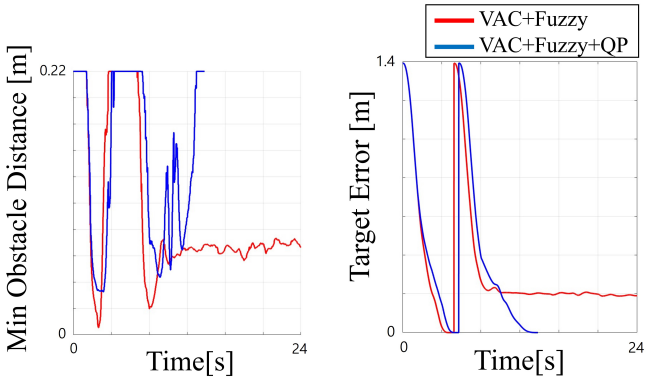

(a) (b)

Fig. 13. (a) Minimum distance to obstacles measured by the sensor, (b) Distance to target point, VAC+fuzzy algorithm failed to overcome the obstacle.

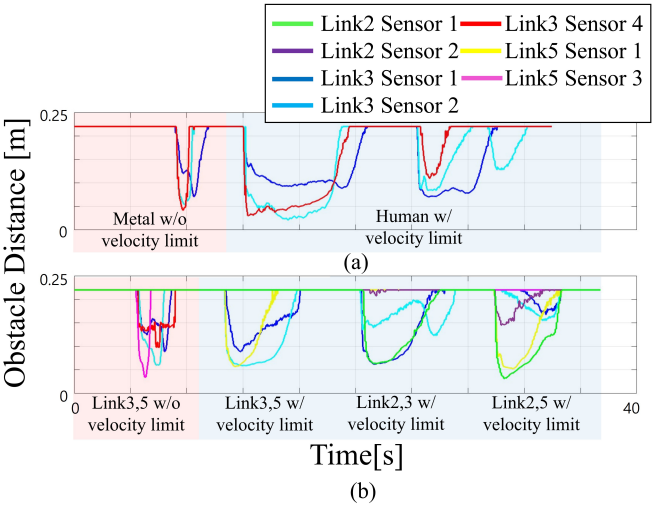

(a)
(b)

Fig. 14. Obstacle avoidance with two dynamic obstacles (a) at one link (b) at two links. Whether there is a velocity limit or not, obstacle avoidance is successful in all cases, with the only difference being the avoidance time.

and soft to the touch. These findings confirm that safe physical interaction between humans and robots can be achieved even during robot motion in real-world environments.

IEEE Robotics and Automation Letters (RA-L) paper, presented at ICRA 2026, Vienna, Austria. Cite as RA-L paper.

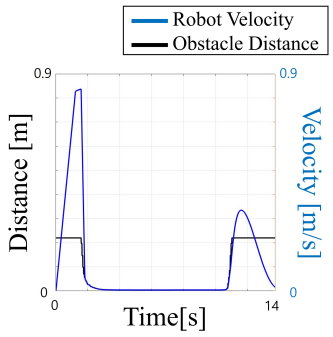

Fig. 15. Robot velocity when the hand touches the robot. When a person makes contact with a robot, the robot's velocity converges to 0 for safe contact.

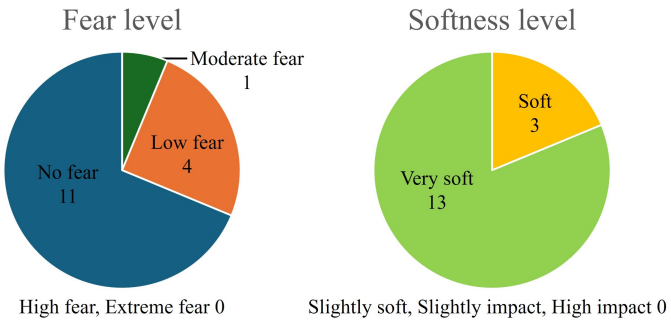

Fig. 16. Investigation of the level of fear and softness when a robot touches a person

VI. Conclusion

This paper presented a safety-critical reactive motion control algorithm for obstacle avoidance and impact mitigation in robotic manipulators using dual-type proximity sensors. The proposed constrained VAC framework dynamically adjusts velocity and impedance parameters in real time while maintaining system passivity via an energy tank mechanism, ensuring safe and stable operation. The framework is robot-agnostic and can be seamlessly integrated into various robotic platforms. It effectively handles both static and dynamic obstacles and, unlike existing methods, enables simultaneous collision avoidance and impact mitigation. Experimental validation on a UR10 robot demonstrated the framework's ability to achieve real-time responsiveness and ensure safe HRI. A key limitation is the lack of global path planning, which will be addressed in future work by integrating motion planning for enhanced trajectory optimization.

References

[1] S. Patil, V. Vasu, and K. V. S. Srinadh, "Advances and Perspectives in Collaborative Robotics: A Review of Key Technologies and Emerging Trends", in *Discover Mechanical Engineering*, vol. 2, 2023. DOI: https://doi.org/10.1007/s44245-023-00021-8.

[2] S. R. Gomez, V. M. Becerra, J. R. Llata, E. G. Sarabia , C. T. Ferrero, and J. P. Oria,"Working Together: A Review on Safe Human-Robot Collaboration in Industrial Environments", in *IEEE Access*, vol. 5, pp. 26754–26773, 2017.

[3] L. Rustler, M. Misar and M. Hoffmann, "Adaptive Electronic Skin Sensitivity for Safe Human-Robot Interaction", in *IEEE-RAS 23rd International Conference on Humanoid Robots (Humanoids)*, pp. 475–482, 2024.

[4] U. Ali, F. Sukkar, A. Mueller, L. Wu, C. Le Gentil, T. Kaupp, and T. Vidal Calleja, "Enabling Safe, Active and Interactive Human-Robot Collaboration via Smooth Distance Fields", in *ACM/IEEE International Conference on Human-Robot Interaction*, pp. 439–446, 2025.

[5] A. Reddy, G. Bright, and J. Padayachee, "A Review of Safety Methods for Human-robot Collaboration and a Proposed Novel Approach", in *International Conference on Informatics in Control, Automation and Robotics*, pp. 243–248, 2019.

[6] P. Francesco and G. G. Paolo, "AURA: An Example of Collaborative Robot for Automotive and General Industry Applications", in *Procedia Manufacturing*, vol. 11, pp. 338–345, 2017.

[7] T. Kim, J. Noh, H. R. Choi, "Development of Flexible Dual-type Proximity Sensor with Resonant Frequency for Robotic Applications", in *IEEE/RSJ International Conference on Intelligent Robots and Systems (IROS)*, 2019.

[8] H. Yim, H. Kang, S. J. Moon, Y. Kim, T. D. Nguyen, H. R. Choi, "Multi-functional safety sensor coupling capacitive and inductive measurement for physical human–robot interaction", in *Sensors and Actuators A: Physical*, vol. 354, pp. 114285, 2023

[9] O. Khatib, "Real-time obstacle avoidance for manipulators and mobile robots", in *IEEE International Conference on Robotics and Automation (ICRA)*, pp. 500–505, 1985.

[10] S. E. Navarro, S. Mühlbacher-Karrer, H. Alagi, H. Zangl, K. Koyama, B. Hein, C. Duriez and J. R. Smith, "Proximity Perception in Human-Centered Robotics: A Survey on Sensing Systems and Applications", in *IEEE Transactions on Robotics (TRO)*, vol. 38, no. 3, pp. 1599–1620, 2022.

[11] S. E. Navarro, S. Koch and B. Hein, "3D contour following for a cylindrical end-effector using capacitive proximity sensors", in *IEEE/RSJ International Conference on Intelligent Robots and Systems (IROS)*, pp. 82–89, 2016.

[12] A. A. Maciejewski and C. A. Klein, "Obstacle avoidance for kinematically redundant manipulators in dynamically varying environments", in *The International Journal of Robotics Research*, vol. 4, no. 3, pp. 109–117, 1985.

[13] Y. Ding and U. Thomas, "Collision avoidance with proximity servoing for redundant serial robot manipulators", in *IEEE International Conference on Robotics and Automation (ICRA)*, pp. 10249–10255, 2020.

[14] K. E. M'Colo, B. Luong, A. Crosnier, C. Néel and P. Fraisse, "Obstacle avoidance using a capacitive skin for safe human-robot interaction", in *IEEE/RSJ International Conference on Intelligent Robots and Systems (IROS)*, pp. 6742–6747, 2019.

[15] Y. Ding and U. Thomas, "Improving safety and accuracy of impedance controlled robot manipulators with proximity perception and proactive impact reactions", in *IEEE International Conference on Robotics and Automation (ICRA)*, pp. 3816–3821, 2021.

[16] S. J. Moon, J. Kim, H. Yim, Y. Kim, H. R. Choi, "Real-Time Obstacle Avoidance Using Dual-Type Proximity Sensor for Safe Human-Robot Interaction", in *IEEE Robotics and Automation Letters*, vol. 6, pp. 8021–8028, 2021.

[17] A. N. Sharkawy, P. N. Koustoumpardis and N. Aspragathos, "A neural network-based approach for variable admittance control in human–robot cooperation: online adjustment of the virtual inertia", in *Intelligent Service Robotics*, vol. 13, pp. 495–519, 2020.

[18] A. N. Sharkawy and P. N. Koustoumpardis, "Human–Robot Interaction: A Review and Analysis on Variable Admittance Control, Safety, and Perspectives", in *Machines*, 2022.

[19] C. H. An and J. M. Hollerbach, "Dynamic Stability Issues in Force Control of Manipulators", in *American Control Conference*, pp. 821–827, 1987.

[20] C. Secchi, S. Stramigioli and C. Fantuzzi, "Control of Interactive Robotic interfaces: a port-hamiltonian approach", in *Springer*, 2007.

[21] F. Ferraguti, N. Preda, A. Manurung, M. Bonfe, O. Lambercy and R. Gassert, "An energy tank-based interactive control architecture for autonomous and teleoperated robotic surgery", in *IEEE Transactions on Robotics*, vol. 31, no. 5, pp. 1073–1088, 2015.

[22] M. Franken, S. Stramigioli, S. Misra, C. Secchi and A. Mac-chelli, "Bilateral telemanipulation with time delays: A two-layer approach combining passivity and transparency", in *IEEE Transactions on Robotics*, vol. 27, no. 4, pp.741 –756, 2011.

[23] C. T. Landi, F. Ferraguti, L. Sabattini, C. Secchi and C. Fantuzzi, "Admittance control parameter adaptation for physical human-robot interaction", in *IEEE International Conference on Robotics and Automation (ICRA)*, pp. 2911–,2916 2017.

[24] F. Dimeas and N. Aspragathos, "Online stability in human-robot cooperation with admittance control", in *IEEE Transactions on Haptics*, vol. 9, no. 2, pp. 267–278, 2016.